

Journal of Materials Chemistry A

Accepted Manuscript



This is an *Accepted Manuscript*, which has been through the Royal Society of Chemistry peer review process and has been accepted for publication.

Accepted Manuscripts are published online shortly after acceptance, before technical editing, formatting and proof reading. Using this free service, authors can make their results available to the community, in citable form, before we publish the edited article. We will replace this *Accepted Manuscript* with the edited and formatted *Advance Article* as soon as it is available.

You can find more information about *Accepted Manuscripts* in the [Information for Authors](#).

Please note that technical editing may introduce minor changes to the text and/or graphics, which may alter content. The journal's standard [Terms & Conditions](#) and the [Ethical guidelines](#) still apply. In no event shall the Royal Society of Chemistry be held responsible for any errors or omissions in this *Accepted Manuscript* or any consequences arising from the use of any information it contains.

ARTICLE

Deposition of Pd/graphene aerogel on nickel foam as a binder free electrode for direct electrooxidation of methanol and ethanol

Cite this: DOI: 10.1039/x0xx00000x

Chi-Him A. Tsang^a, K.N. Hui^{*b}, K.S. Hui^{*c} and L. Ren^dReceived 00th January 2012,
Accepted 00th January 2012

DOI: 10.1039/x0xx00000x

www.rsc.org/

We reported a simple and green method to fabricate different palladium (0.8, 2.17, 7.65 wt.%) loaded graphene aerogel deposited on nickel foam (Pd/GA/NF) as binder-free direct electrodes for electrooxidation of methanol and ethanol. L-ascorbic acid (vitamin C, VC) was used as a reducing agent in the process under a mild temperature of 40 °C. The morphology, chemical composition, and electrochemical performance of the prepared electrodes were characterized by optical microscopy, SEM/EDX, TEM, XRD, XPS, XRF, and cyclic voltammetry (CV), respectively. The XPS results revealed that both graphene oxide and Pd ions were reduced simultaneously by VC. The CV analysis revealed that the 7.65 wt.% Pd/GA/NF electrode showed a maximum peak current density of 798.8 A g⁻¹ (forward to backward peak current density ratio (I_f/I_b) of 3.11), and 874 A g⁻¹ (I_f/I_b of 2.72) in methanol and ethanol electrooxidation, respectively. The catalytic performance of the electrodes was enhanced with increasing the Pd loading. The results indicated that the 7.65 wt.% Pd/GA/NF electrode exhibited a good electrocatalytic activity and an outstanding stability in alcohol electrooxidation. The prolong CV scanning study (over 1000 cycles) showed that the 7.65 wt.% Pd/GA/NF electrode achieved a better overall performance and stability in ethanol oxidation compared to methanol oxidation. The proposed electrode preparation method has a great potential for preparing various binder-free catalytic electrodes, which would be beneficial to the development of fuel cell application.

Introduction

Fuel cell is one of the most effective devices for energy conversion with low pollution characteristics.¹ Direct methanol fuel cell (DMFC) and direct ethanol fuel cell (DEFC) have been widely investigated because of high energy conversion efficiency, low operation temperature, low pollutant emission, ease of storage, low cost, and ease of handling.²⁻⁵ Pt and Pd are the most commonly used catalysts in DMFC/DEFC due to their strong electrocatalytic activity in oxidation of alcohol.^{1-3, 6-8} However, the problems of high cost, low abundance and catalytic poisoning by the carbon monoxide produced in electrooxidation have severely restricted the practical usage of Pt-based electrocatalyst. Alternatively, Pd has become the focus of electrocatalyst for DMFC or DEFC as it is relatively low cost, higher abundance, and more difficult to be poisoned by the carbon monoxide generated in the electrooxidation of alcohol.^{1-3, 9-10}

Recently, due to its unique electrical, mechanical, optical, and thermal properties, reduced graphene oxide has become a promising materials for different applications in various field such as energy, catalysis, and sensing.^{2, 11-19} The abundant functional groups on the surface of graphene oxide (GO) provide many favorable sites for anchoring various metal nanoparticles in graphene.¹² Graphene aerogel (GA), the presence of 3D cross-linked network of graphene nanosheets, has become a new focus as it is an ideal prototype for

maximizing the accessible surface areas for photocatalysis and electrocatalysis.¹⁴ To date, metal loaded GA was prepared by thermal reduction of metal ions and GO mixture through hydrothermal reaction, followed by freeze drying of the as-prepared hydrogel.^{2-3, 11-13, 20-21} However, hydrazine and harsh conditions are commonly used in the reported methods, which made it environmentally unfriendly.^{2, 11-13, 20-21} Very recently, a green and friendly pathway of nanoparticle/graphene composites, utilizing a mild reducing agent such as L-ascorbic acid (vitamin C; VC) under low temperature condition, was developed by some research groups.^{11, 14, 22-24}

Binder-free electrodes have been drawn a large attention due to its convenience and no-binder feature in various electrochemical applications, like lithium ion battery, supercapacitor and electrocatalysis.²⁵⁻²⁷ Although binder-free graphene-based fuel cell electrodes were developed with different methods, 2D graphene sheets were loaded on the substrates.^{8, 28} Very recently, an one-step preparation of 3D GA on small piece of porous nickel foam (NF) was reported, which showed a huge potential application as binder-free electrodes for supercapacitor.²⁵⁻²⁶ However, to the best of our knowledge, there is no report about a simple method to prepare palladium loaded GA on nickel foam (Pd/GA/NF) as binder-free direct electrodes for electrooxidation of methanol and ethanol.

In view of great potential applications of Pd/GA/NF electrodes in electrocatalytic oxidation, herein, we reported a simple and green method to prepare binder-free Pd/GA/NF

electrodes with different Pd loadings for alcohol electrooxidation. The Pd/GA/NF electrodes were formed through the self-assembly aggregation of Pd/GA on NF during the reduction of GO and Pd ions by non-toxic reducing agent VC at 40 °C. The morphology, chemical composition, and electrochemical performance of the prepared electrodes were characterized by optical microscopy, SEM/EDX, TEM, XRD, XPS, XRF, and cyclic voltammetry (CV), respectively. The results indicated that the 7.65 wt.% Pd/GA/NF electrode exhibited a good electrocatalytic activity and an outstanding stability in alcohol electrooxidation.

Experimental

Materials

The porous Ni foam (NF; 110 pore per inch; mass density of 320 g m⁻²; Artenano Company Limited, Hong Kong), potassium hexachloropalladate (IV) (K₂PdCl₆, 99.9999%, Sigma-Aldrich), methanol (MeOH, 99.9%, Sigma-Aldrich), ethanol (EtOH, absolute, Sigma-Aldrich), vitamin C (VC; Hwa Da Chemical), and potassium hydroxide (KOH, 85%, Sigma-Aldrich) were used directly as received. All aqueous solutions were prepared with Milli-Q water.

Preparation of Pd/GA/NF electrodes

The GO was prepared through the modified Hummer's method.²³ The Pd/GA deposited on the NF was prepared at a low temperature 40 °C compared to the published work.¹⁴ Briefly, 120 mg of freeze dried GO was dispersed in 20 ml DI water for few minutes in order to produce 6 mg ml⁻¹ GO dispersion. Different amounts of K₂PdCl₆ (8, 16, and 80 mg) were added to the GO dispersion and stirred constantly at room temperature for 30 min in order to obtain the well mixed PdCl₆²⁻/GO mixture (with Pd⁴⁺ ions of 1, 5, and 10 mM). The cleaned porous NF strip (10 cm × 0.5 cm × 0.2 cm) was immersed into the PdCl₆²⁻/GO dispersion with ultrasonic treatment for 20 min, followed by aging at room temperature for 2 h. The PdCl₆²⁻/GO soaked NF was then transferred to a bottle containing 0.5 g VC (143 mM, 20 ml) solution and left stationary at 40 °C for 24 h in order to facilitate the formation of Pd/graphene hydrogel on NF (Pd/GH/NF). The prepared Pd/GH/NF electrodes were cleaned by soaking the strip in DI water for 3 days in order to remove the residue VC and Pd⁴⁺ ions. The cleaned Pd/GH/NF electrodes were freeze dried for 48 h at -80 °C under vacuum to produce the Pd/GA/NF electrodes. The roles of GA are to (1) disperse Pd NPs on its surface to prevent the NPs from agglomeration during electrooxidation of methanol and ethanol, and (2) enhance the conductivity of the electrodes in electrooxidation of methanol and ethanol. Based on the XRF analysis, 0.8 wt.% Pd/GA/NF electrode (0.8 wt.% Pd was loaded in the electrode) was produced, which was prepared with 1 mM PdCl₆²⁻ ions in the process. Similarly, 2.17 wt.% Pd/GA/NF, and 7.65 wt.% Pd/GA/NF electrodes were produced, which were prepared with 5 mM, and 10 mM PdCl₆²⁻ ions in the synthesis, respectively. A GA/NF electrode was also prepared by the same way without the addition of K₂PdCl₆.

Characterization

The optical image of the electrodes was obtained by using a stereo microscope (Olympus SZX12). The SEM/EDX analysis of the electrodes was conducted using a SEM system (JEOL-JSM5600). The TEM analysis was conducted through a

TEM system (Philips CM20) operated at accelerating voltage of 20 kV. Pd NPs size was analyzed through the evaluation of a set of randomly selected particles (80-150 NPs) of different regions in the typical TEM images. The bulk elemental composition of the electrodes was determined by an Eagle III X-Ray Fluorescence spectrometer (EDAX-Eagle III). The surface elemental composition of the electrodes was determined by X-ray photoelectron spectroscopy (XPS, Physical Electronics PHI 5802). The C1s signal at 285 eV was utilized for making appropriate charging effect corrections. The accuracy of the absolute concentration for each element was within ±10%. Powder X-ray diffraction (XRD) patterns of the GA and the Pd/GA samples (removed from each electrode) were obtained using a powder diffractometer (Philips Xperts') equipped with a Cu-Kα radiation. Thus, Ni peak was not observed in the XRD results. The accelerating voltage and current used were 40 kV and 20 mA, respectively. The scanning range of 2θ was set between 5 and 95°, with a step size of 0.02° and 0.01° s⁻¹.

Electrochemical characterization of Pd/GA/NF electrodes

The electrochemical characterization of the electrodes was performed by CHI660D electrochemical workstation with conventional 3-electrode system.^{8-9, 19, 29-30} A three-electrode cell system has been commonly used to evaluate the fuel cell electrodes. Freeze dried Pd/GA/NF electrodes were used as a working electrode without further treatment. A standard calomel electrode (SCE: HgCl₂/Hg), and a Pt wire were used as a reference, and a counter electrodes, respectively. The electrolytes were 1 M MeOH/1 M KOH and 1 M EtOH/1 M KOH solutions for the DMFC and the DEFC measurements, respectively. The scanning rate of the system was set at 0.05 V s⁻¹, and the scanning range was -0.845 to +0.355 V, and -0.845 to +0.955 V against SCE for DMFC and DEFC measurements, respectively.^{3, 7} The current density, J_r, was defined as the normalized value of current with respect to Pd by dividing the absolute current from the redox peak in CV scan by the effective mass of Pd (0.4 mg) in the electrodes. The average values of three sets of independent experiments (deviations within ±5%) were reported using three different batches of the samples.

Results and discussions

Characterization of Pd/GA/NF electrodes

Fig. 1 shows the typical SEM images of NF and the 7.65 wt.% Pd/GA/NF electrode with its EDX spectrum. The NF is composed of macroscopic 3D porous structure with layer cross-linked grid structure (Fig. 1a).³¹⁻³² In Figs. 1b-1c, Pd/GA was deposited on the NF surface and partially filled into the NF pores, which reflected that the PdCl₆²⁻/GO dispersion was covered on the NF surface during the aging step. Such result was coherent to the digital images and stereo microscope images of the sample (Fig. S1). In Fig. 1d, some particles were observed on surface of GA, which was confirmed to be Pd element by the EDX spectrum (Fig. 1e). The Ni peak observed in the spectrum was due to the background signal from the NF.

According to the XRF results, different amounts of Pd were loaded in the electrodes. The amount of Pd (wt.%) loaded in the electrodes increased with increasing initial concentration of PdCl₆²⁻ ions in synthesis. Figs. 2a-2c show the SEM images of Pd/GA coated on different electrodes. More Pd NPs were loaded on the surface of GA of the electrodes with increasing initial concentration of PdCl₆²⁻ ions in the synthesis. TEM

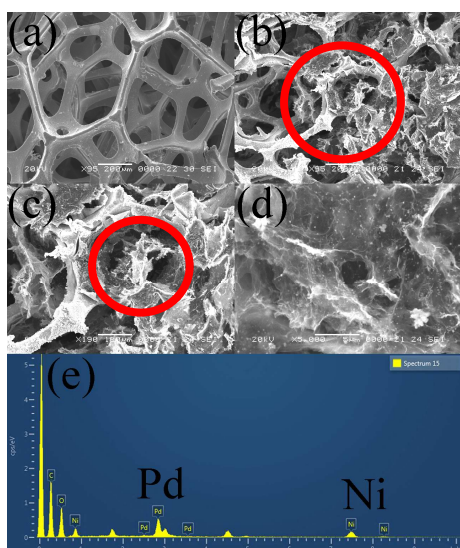


Fig. 1 SEM images of (a) NF, (b) 7.65 wt.% Pd/GA/NF (95 \times , scale bar: 200 μ m), (c) magnified image of red circle area of (b) (190 \times , scale bar: 5 μ m), (d) magnified image of red circle area of (c) (5000 \times , scale bar: 2 μ m), and (e) EDX spectrum of 7.65 wt.% Pd/GA/NF.

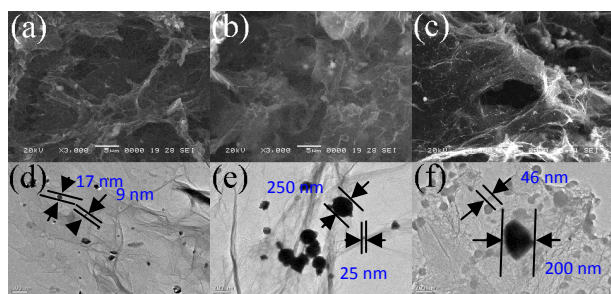


Fig. 2 SEM images (scale bar: 5 μ m) of (a) 0.8 wt.% Pd/GA/NF, (b) 2.17 wt.% Pd/GA/NF, (c) 7.65 wt.% Pd/GA/NF, and TEM images of (d) 0.8 wt.% Pd/GA/NF (scale bar: 100 nm), (e) 2.17 wt.% Pd/GA/NF (scale bar: 200 nm), (f) 7.65 wt.% Pd/GA/NF (scale bar: 200 nm).

images (Figs. 2d-2f and S2-S4) show that the size of Pd NPs was increased from the range of 9-17 nm (in 0.8 wt.% Pd/GA/NF) to the range of 46-200 nm (in 7.65 wt.% Pd/GA/NF). The average size of Pd NPs was 34.1 nm (in 0.8 wt.% Pd/GA/NF), 164.3 nm (in 2.17 wt.% Pd/GA/NF), and 133.6 nm (in 7.65 wt.% Pd/GA/NF). The increase of size of Pd NPs was due to higher nucleation rate of Pd ions in the synthesis under higher concentration of PdCl₆²⁻ ions.³³⁻³⁴

Fig. 3 shows the XRD patterns of the GA and the Pd/GA powders which were removed from the electrodes. The position of Pd 2 θ peaks at 40 $^\circ$, 47 $^\circ$, 68 $^\circ$, 82 $^\circ$ are assigned to the Pd (111), Pd (200), Pd (220) and Pd (311), respectively.^{11,13} The results indicate that Pd NPs have the f-c-c structure (JPCDS card No. 46-1043) with high crystallinity. The Pd (111) peak intensity was increased with increasing Pd loading in the electrodes. The result indicated that Pd ions were reduced to metallic Pd by VC in the synthesis. No 2 θ diffraction peaks of Ni element are observed in the XRD patterns.²⁰ Moreover, carbon diffraction peaks are observed at 11.85 $^\circ$ and 26 $^\circ$ of the Pd/GA powder samples, corresponding to the presence of amorphous carbon in

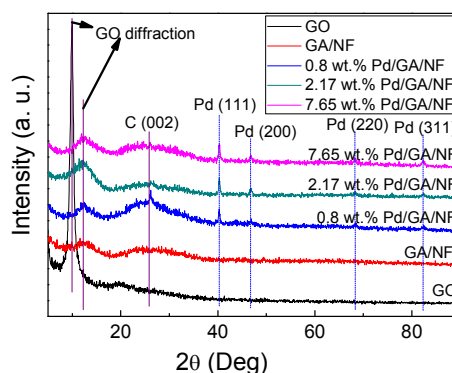


Fig. 3 XRD patterns of the GA and the Pd/GA powders which were removed from the electrodes.

the GA. Comparing with the graphite oxide peak recorded at 10 $^\circ$ in the GO, the interlayer distance between the graphene nanosheets was reduced from 8.84 \AA in the GO to 7.46 \AA in the GA, which was due to the existence of π - π stacking between graphene sheets.³⁵ The result indicated that GO was reduced to GA in the synthesis.

Fig. 4a-4c shows the elemental composition of the 7.65 wt.% Pd/GA/NF electrode by XPS analysis. In Fig. 4a, Ni remained in the form of metallic Ni or NiO in the electrode. There was no Ni-C signal from both C1s and Ni 2p_{3/2} spectra. In Fig. 4b, the strong signals at 335.2 eV and 340.4 eV were corresponded to Pd⁰, and the weak signals at 337.3 eV and 342.6 eV (shoulder peaks) were corresponded to Pd²⁺.^{2, 36-37} The results indicated that Pd NPs were loaded in GA with traces amount of Pd²⁺ existed in the electrode. The traces amount of Pd²⁺ ions were expected to play a role in maintaining a strong mechanical integrity of the GA structure, as suggested by our previous work.³⁸ In Fig. 4c, signals at 284.3, 286.1 (shoulder peak), 288.3 and 288.8 (shoulder peak) eV were observed, which were assigned to C-C, -C-OH, -O-C-O-, and O=C-OH groups, respectively.² The intensity of oxide functional groups was strongly reduced after the synthesis by comparing to the C1s spectrum of GO (Fig. 4d). The finding is similar to the GA products obtained from other reducing agents such as NaBH₄ and hydrazine.^{22, 25-26}

Electrochemical oxidation ability of Pd/GA/NF

Fig. 5a shows the CV curves of NF, GA/NF, and Pd/GA/NF electrodes in the 25th cycle of methanol oxidation. No redox peak was observed in NF, GA/NF, and the 0.8 wt.% Pd/GA/NF electrodes. The 25th cycles were used due to the shape of the CV curves of each electrode (from the 25th to 50th cycles) did not significantly changed, which allows for clear comparison. The results indicated that Ni and GA were not active in methanol oxidation. The results also indicated that 0.8 wt.% of Pd in the electrode was not high enough to initiate an observable methanol oxidation. In forward scan, shifting of anodic peaks from +0.24 V (2.17 wt.% Pd/GA/NF) to +0.18 V (7.65 wt.% Pd/GA/NF) towards negative potential was observed with increasing Pd loading in the electrodes. Based on the SEM and TEM analyses (Figs. 2 and S2-S4), the morphology of Pd NPs were similar in the electrodes. However, the size and the coverage of Pd NPs on GA was increased in the 7.65 wt.% Pd/GA/NF. Shifting of anodic peak may be due to better interaction between Pd NPs and methanol molecules in

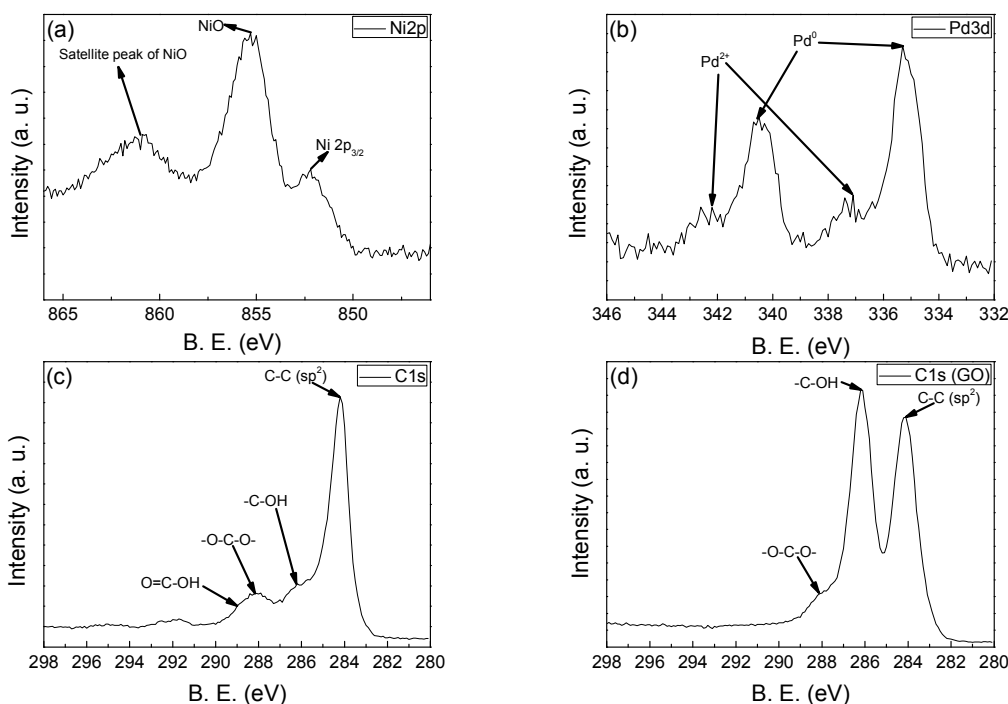


Fig. 4 XPS spectra of (a) Ni2p, (b) Pd3d, and (c) C1s in 7.65 wt.% Pd/GA/NF, and (d) C1s of GO.

the 7.65 wt.% Pd/GA/NF. It should be noted that the shift in the oxidation wave is also dependent on the porosity of the aerogel support and therefore the proportion of active Pd clusters that are situated on the surface or within pores. Thus, the oxidation wave may move due to the mass transport effects, which will be investigated in our ongoing work. Fig. 5b showed that the onset potential of the electrodes was also shifted to negative potential from -0.38 V (2.17 wt.% Pd/GA/NF) to -0.50 V (7.65 wt.% Pd/GA/NF), which indicated that the kinetics of electrocatalytic reactions was enhanced with increasing the Pd loading in the electrodes.⁶ The onset potential of the electrodes was estimated from the intersection point of 2 tangents produced from the turning point line and the baseline of the forward scan redox peak in the CV curve.³⁹ With the 2.17 wt.% Pd/GA/NF electrode, an anodic peak of J_f value of 187.3 A g^{-1} (at +0.24 V) and a cathodic peak of J_b value of 72.4 A g^{-1} (at -0.21 V) were observed, which were ascribed to methanol oxidation by Pd NPs in the electrode, and reduction of PdO to Pd or removal of incompletely oxidized carbon species formed on the surface of Pd NPs in the forward scan, respectively.^{2,7} The corresponding peak current ratio (I_f/I_b) of 2.58 was calculated, which reflects the tolerance of the electrode against the poisoning in electrooxidation of methanol. Increasing Pd loading from 2.17 wt.% to 7.65 wt.% in the electrodes, the value of J_f , J_b , and I_f/I_b was increased to 788 A g^{-1} , 259.5 A g^{-1} , and 3.03, respectively. The results indicated that amount of Pd in the electrode influenced the rate of methanol oxidation and the tolerance ability of the electrode against the poisoning.

Fig. 5c shows the CV curves of NF, GA/NF, and Pd/GA/NF electrodes in the 25th cycle of ethanol oxidation. No redox peak was observed in both NF and GA electrodes, which reflected that Ni and GA was not active ingredient in ethanol oxidation. An anodic peak (+0.08 V) was observed in the 0.8 wt.% Pd/GA/NF electrode. Increasing Pd loading in the

electrodes, the anodic peak was shifted towards positive potential from +0.08 V (0.8 wt.%) to +0.43 V (2.17 wt.%), and further increased to +0.57 V (7.65 wt.%), as shown in Fig. 5c. It was reported that shifting of anodic peak in ethanol electrooxidation was related to the Pd NPs morphology under the same scanning rate (0.05 V s^{-1}).⁴⁰ The morphology of Pd NPs could reduce the energy barrier between Pd NPs and ethanol molecules. However, similar morphology of Pd NPs were observed in the Pd/GA/NF electrodes (Figs. 2 and S2-S4). The results indicated that the shift of anodic peak was due to the increase of the particle size and the density of Pd NPs loaded in the electrodes. The mass transport effect of the electrodes may be another possible reason for such phenomenon, which will be investigated in our going work. Fig. 5d shows that the onset potential was gradually shifted to more negative region from -0.50 V (0.8 wt.%) to -0.62 V (2.17 wt.%), and finally to -0.60 V (7.65 wt.%), which reflected that the kinetics of ethanol oxidation was enhanced when Pd loading in the electrodes was increased from 0.8 wt.% to 2.17 wt.%, and then slightly reduced when Pd loading in the electrodes was further increased to 7.65 wt.%. With the 0.8 wt.% Pd/GA/NF electrode, J_f value of 393.7 A g^{-1} (+0.08 V), and J_b value of 157.3 A g^{-1} (-0.36 V) were observed. Increasing Pd loading to 2.17 wt.% in the electrode, the J_f and J_b values were increased to 914.7 A g^{-1} (+0.38 V) and 464.5 A g^{-1} (-0.21 V), respectively, which was due to higher Pd loading in the electrode.^{1, 41} However, the J_f and J_b values were reduced to 744.3 A g^{-1} (+0.57 V) and 343.8 A g^{-1} (-0.18 V) when Pd loading was further increased to 7.65 wt.%. It may be due to the agglomeration of Pd NPs in the electrode.¹ Increasing the Pd loading in the electrodes, the I_f/I_b ratio was first decreased from 2.58 (0.8 wt.% Pd/GA/NF) to 1.97 (2.17 wt.% Pd/GA/NF), then was increased to 2.17 (7.65 wt.% Pd/GA/NF).

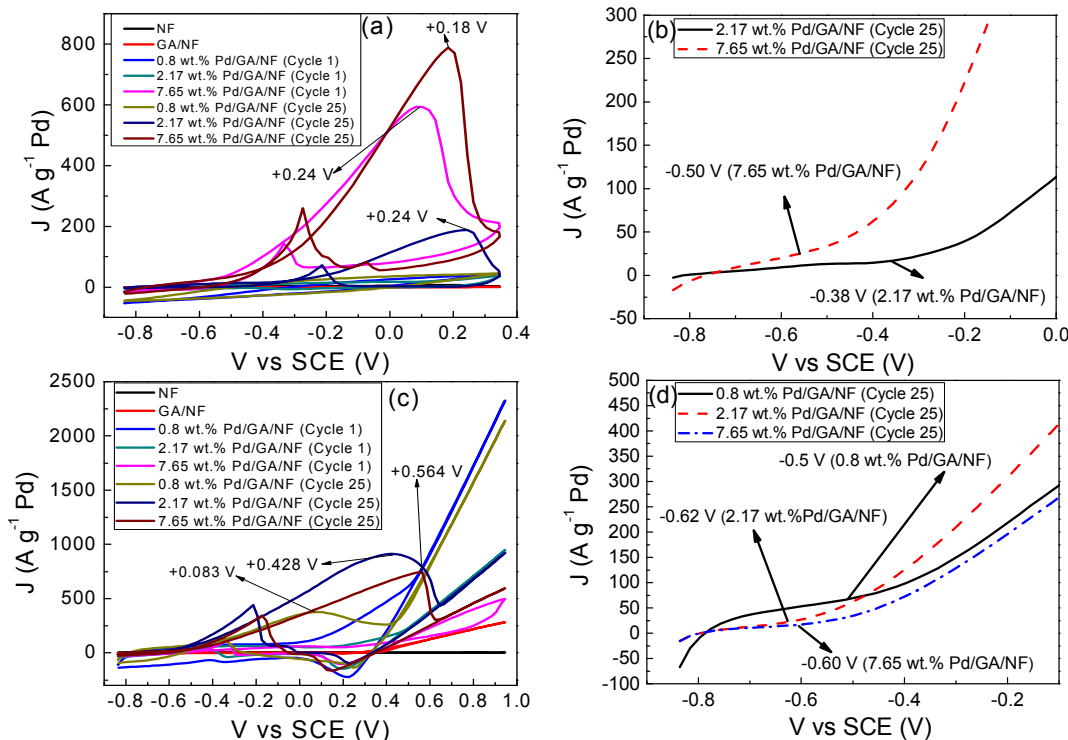


Fig. 5 CV of NF, GA/NF, and the Pd/GA/NF electrodes in (a) 1 M MeOH/1 M KOH solution (-0.845 to +0.355 V), (b) zoom portion (-0.845 to 0 V) of (a), (c) 1 M EtOH/1 M KOH solution (-0.845 to +0.955 V), and (d) zoom portion (-0.845 to -0.1 V) of (c).

The electrocatalytic stability of the 2.17 wt.% Pd/GA/NF (as shown in Fig. S5) and the 7.65 wt.% Pd/GA/NF electrodes (as shown in Fig. 6b) in ethanol oxidation was first evaluated in 1000 cycles. For the 2.17 wt.% Pd/GA/NF and the 7.65 wt.% Pd/GA/NF, J_f were first remained unchanged in 25-100 cycles, and then dropped dramatically to 20% of the maximum value after 1000 cycles. In the 1000th cycles, the I_f/I_b ratio of 7.65 wt.% Pd/GA/NF electrode (2.17) was higher than that of 2.17 wt.% Pd/GA/NF electrode (1.97). The results reflected that 7.65 wt.% Pd/GA/NF electrode is relatively stable in a long operation. In the following tests, 7.65 wt.% Pd/GA/NF electrode was selected.

Ni has been considered as an electrocatalyst for electrooxidation of alcohol.²⁰ To clarify the influence of Ni on oxidation of alcohols, CV scans of NF, GA/NF, and 7.65 wt.% Pd/GA/NF electrodes in 1 M MeOH/1 M KOH (Fig. S6a) was performed in the range of -0.245 to +0.955 V (vs SCE) which was the active potential of Ni driven electrooxidation of methanol. In Figs. S6a and 5, no Ni catalyzed alcohol electrooxidation redox peaks were observed in the CV curves of the GA/NF and the 7.65 wt.% Pd/GA/NF electrodes. However, a weak Ni^{2+}/Ni^{3+} redox peak (+0.2 V) in the reverse scan of ethanol oxidation (Figs. 5c and S6c) was observed compared with the CV curve of NF (Figs. S6b and S6d).²⁰ The results reflected that Pd was the major active species in alcohol electrooxidation.

Fig. 6a shows that the CV curves of 7.65 wt.% Pd/GA/NF electrode in methanol electrooxidation over 1000 cycles (total reaction time is 13 h and 20 min). The corresponding J_f , J_b , I_f/I_b ratio, and onset potential were summarized in Table S1 and Fig.

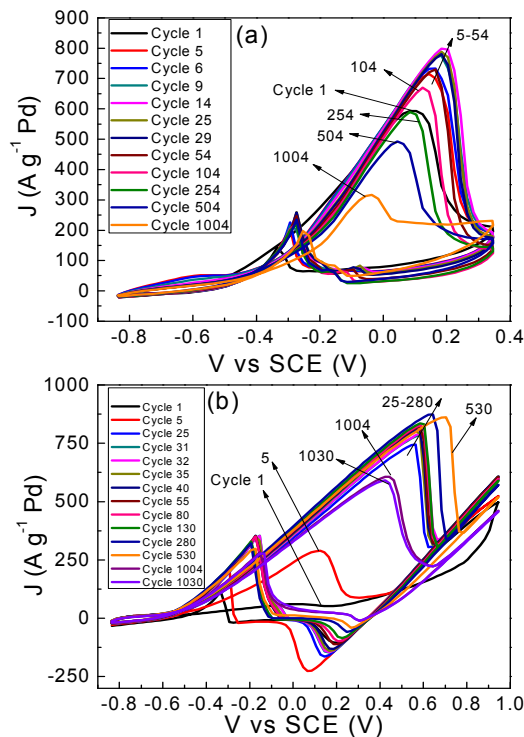


Fig. 6 CV of 7.65 wt.% Pd/GA/NF in (a) 1 M MeOH/1 M KOH solution (-0.845 to +0.355 V), and (b) 1 M EtOH/1 M KOH solution (-0.845 to +0.955 V) over 1000 scans.

7. The J_f of the anodic peak in forward scan was continuously increased from the 1st cycle to 14th cycle, then it was significantly decreased up to the 1000th cycle (~60% of reduction). The increase of J_f in the 14th cycle was due to the activation of the electrode for methanol oxidation. Then, the decrease of J_f in the 14th to 1000th cycles was resulted from the deactivation of the electrode which may be due to the poisoning by the intermediate species formed.³¹ The tolerance ability of the electrode was reflected in Fig. 7b, which is similar to the trend of variation of J_f . Fig. 7c shows the trend of variation of the onset potential of the electrode. The onset potential was shifted to a negative potential (-0.536 V) in the 29th cycle, and then stabilized at -0.496 V in the 1004th cycle. The result indicated that a maximum kinetics of methanol oxidation was observed in the 29th cycle.

Fig. 6b shows that the CV curves of 7.65 wt.% Pd/GA/NF electrode in ethanol electrooxidation over 1000 cycles (total reaction time is 20 h and 36 min). The corresponding J_f , J_b , I_f/I_b ratio, and onset potential were summarized in Table S2 and Fig. 7. The J_f of the anodic peak in forward scan was continuously increased from the 1st cycle to the 280th cycle, then was stabilized up to the 530th cycle, and finally decreased up to the 1030th cycle (~32% of reduction). The increase of J_f in the 280th cycle was due to the fully activation of the electrode for ethanol oxidation. Then, the decrease of J_f in the 530th to the 1030th cycles was resulted from the deactivation of the electrode which may be due to the poisoning of Pd catalyst.³¹ The tolerance ability of the electrode was reflected in Fig. 7b, which is similar to the trend of variation of J_f . Compared to methanol oxidation, the results indicated that the electrode achieved a strong tolerance towards poisoning in the first 530th cycles. Fig. 7c shows the trend of variation of the onset potential of the electrode. The onset potential was shifted to a negative potential (-0.636 V) in the 530th cycle, and then stabilized at -0.616 V in the 1030th cycle. The result indicated that the kinetics of ethanol oxidation was maintained over the 1000th cycle. Based on the results of Figs. 6 and 7, it indicated that the 7.65 wt.% Pd/GA/NF electrode performed better in ethanol oxidation in terms of current density, tolerance ability, and stability.

Table S3 compares the best values of peak current density, and tolerance ability of the current electrodes with some reported electrocatalysts. The peak current density of the 7.65 wt.% Pd/GA/NF electrode is approximately 1.5 times (MeOH) and 6.1 times (EtOH) higher than the reported values in literature.^{6,43} The I_f/I_b ratio value recorded in this work was laid between that of Pd/CNT (<1) and Pd-RGO (6.05) for methanol oxidation,^{6,43} and Pd/Nafion-graphene/GCE (4.0) and Pd/C (0.7) for ethanol oxidation.^{3,43-44} The findings indicated that the 7.65 wt.% Pd/GA/NF electrode processed satisfactory tolerance to catalytic poisoning in methanol and ethanol electrooxidation.³ The enhanced electrocatalytic activity may benefit from nanosized Pd NPs embedded in the 3D porous GA structure. The 3D porous GA framework deposited on the NF surface can enhance effective mass transfer of reactants to the active sites for oxidation. Table 1 further compares the values of peak current density and tolerance ability of the current electrodes at the 1000th cycle with some reported electrocatalysts. The results indicated that the 7.65 wt.% Pd/GA/NF electrode outperformed other Pd based electrocatalysts in a long operation.^{9,31,42} The results indicated that the Pd/GA/NF electrodes have high tolerance against poisoning in methanol and ethanol oxidation.

Table 1 Comparison of current density (J_f) in the anodic scan and I_f/I_b ratio of some Pd based electrocatalyst for methanol and ethanol oxidation.

| Catalyst | J_f (MeOH/ KOH) | J_f (EtOH/ KOH) | I_f/I_b (MeO H) | I_f/I_b (EtO H) | Refere nce electro de | Ref |
|-----------------------|--|---|-------------------------|-------------------------|--------------------------------|--------------|
| Anodized Pd | 76.8 (A g ⁻¹ Pd) (200 th cycle) | N/A | 1.41 | N/A | RHE | 42 |
| Pd/NF | N/A | 105.7 (mA cm ⁻¹) (500 th cycle) | N/A | N/A | MMO | 31 |
| Pd/LDH- NWs | N/A | 1.93 (mA cm ⁻²) (500 th cycle) | N/A | 1.01 | MMO | 9 |
| 2.17 wt.% Pd/GA/NF | 197.1 (A g ⁻¹ Pd) (1000 th cycle) | 300 (A g ⁻¹ Pd) (1000 th cycle) | 1.77 | 1.95 | SCE | This work |
| 7.65 wt.% Pd/GA/NF | 316 (A g ⁻¹ Pd) (1004 th cycle) | 590.2 (A g ⁻¹ Pd) (1030 th cycle) | 1.61 | 2.13 | SCE | This work |

Conclusions

We reported a simple and green method to fabricate different palladium (0.8, 2.17, 7.65 wt.%) loaded graphene aerogel deposited on nickel foam (Pd/GA/NF) as binder-free direct electrodes for electrooxidation of methanol and ethanol. The results indicated that the Pd/GA/NF electrodes exhibited a satisfactory performance in methanol and ethanol electrooxidation in alkaline media. The amount of Pd in the electrode influenced the rate of methanol/ethanol oxidation and the tolerance ability of the electrode against the poisoning. The 7.65 wt.% Pd/GA/NF electrode exhibited a better performance in ethanol oxidation. High electrocatalytic activity of the 7.65 wt.% Pd/GA/NF electrode was due to a higher loading of Pd and a good dispersion of nanosized Pd NPs embedded in the 3D porous GA deposited on the NF. The proposed electrode preparation method has a great potential for preparing various binder-free catalytic electrodes, which would be beneficial to the development of fuel cell devices.

Acknowledgements

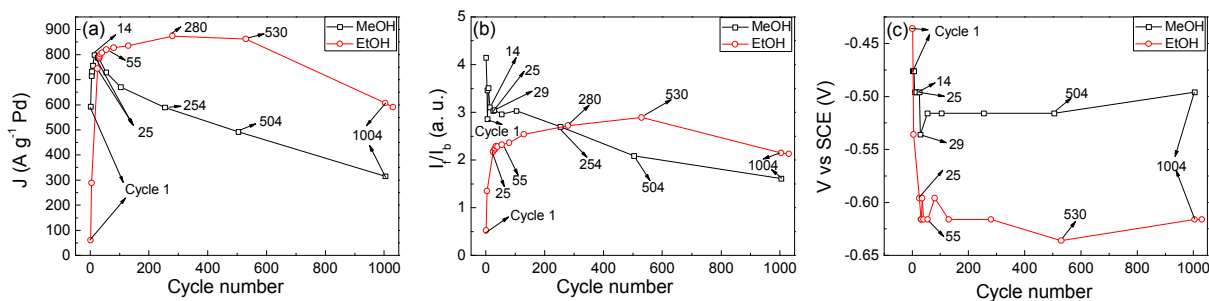


Fig. 7 Variation of (a) J_F , (b) I_F/I_b , and (c) onset potential of the 7.65 wt.% Pd/GA/NF in methanol and ethanol oxidation.

This work was supported by the research fund of Hanyang University (HY-2013 year), and the Basic Science Research Program through the National Research Foundation of Korea (NRF) funded by the Ministry of Education, Science and Technology (2013R1A1A2007365).

Notes and references

^a Department of System Engineering and Engineering Management, City University of Hong Kong, Hong Kong

^b School of Materials Science and Engineering, Pusan National University, San 30 Jangjeon-dong, Geumjeong-gu, Busan 609-735, Republic of Korea

^c Department of Mechanical Convergence Engineering, Hanyang University, 17 Haengdang-dong, Seongdong-gu, Seoul 133-791, Republic of Korea

^d Faculty of Materials and Optoelectronic physics, Xiangtan University, Hunan 411105, P. R. China

† Electronic Supplementary Information (ESI) available: [details of any supplementary information available should be included here] See DOI: 10.1039/b000000x/

- J. Yang, C. Tian, L. Wang and H. Fu, *J. Mater. Chem.*, 2011, **21**, 3384-3390.
- H. J. Huang and X. Wang, *J. Mater. Chem.*, 2012, **22**, 22533-22541.
- X. Yang, Q. D. Yang, J. Xu and C. S. Lee, *J. Mater. Chem.*, 2012, **22**, 8057-8062.
- Z. Ozturk, F. Sen, S. Sen and G. Gokagac, *J. Mater. Sci.*, 2012, **47**, 8134-8144.
- N. Arjona, M. Guerra-Balcazar, F. M. Cuevas-Muniz, L. Alvarez-Contreras, J. Ledesma-Garcia and L. G. Arriaga, *RSC Adv.*, 2013, **3**, 15727-15733.
- F. C. Zhu, G. S. Ma, Z. C. Bai, R. Q. Hang, B. Tang, Z. H. Zhang and X. G. Wang, *J. Power Sources*, 2013, **242**, 610-620.
- R. S. Li, H. Mao, J. J. Zhang, T. Huang and A. S. Yu, *J. Power Sources*, 2013, **241**, 660-667.
- T. Maiyalagan, X. C. Dong, P. Chen and X. Wang, *J. Mater. Chem.*, 2012, **22**, 5286-5290.
- J. W. Zhao, M. F. Shao, D. P. Yan, S. T. Zhang, Z. Z. Lu, Z. X. Li, X. Z. Cao, B. Y. Wang, M. Wei, D. G. Evans and X. Duan, *J. Mater. Chem. A*, 2013, **1**, 5840-5846.
- X. L. Yang, X. Y. Wang, X. Z. Liu, Y. J. Zhang, W. G. Song, C. Y. Shu, L. Jiang and C. R. Wang, *J. Mater. Chem. A*, 2013, **1**, 8332-8337.

- S. H. Kim, G. H. Jeong, D. Choi, S. Yoon, H. B. Jeon, S. M. Lee and S. W. Kim, *J. Colloid Interf. Sci.*, 2013, **389**, 85-90.
- J. Li, C.-y. Liu and Y. Liu, *J. Mater. Chem.*, 2012, **22**, 8426-8430.
- G. H. Jeong, S. H. Kim, M. Kim, D. Choi, J. H. Lee, J. H. Kim and S. W. Kim, *Chem. Commun.*, 2011, **47**, 12236-12238.
- Z. Sui, X. Zhang, Y. Lei and Y. Luo, *Carbon*, 2011, **49**, 4314-4321.
- Y. Zhu, S. Murali, M. D. Stoller, K. J. Ganesh, W. Cai, P. J. Ferreira, A. Pirkle, R. M. Wallace, K. A. Cychosz, M. Thommes, D. Su, E. A. Stach and R. S. Ruoff, *Science*, 2011, **332**, 1537-1541.
- Y. J. Gao, D. Ma, C. L. Wang, J. Guan and X. H. Bao, *Chem. Commun.*, 2011, **47**, 2432-2434.
- Z. Jin, D. Nackashi, W. Lu, C. Kittrell and J. M. Tour, *Chem. Mater.*, 2010, **22**, 5695-5699.
- S. Chen, J. W. Zhu, L. Qiu, D. Li and X. Wang, *Chem.-Eur. J.*, 2013, **19**, 7631-7636.
- X. L. Yang, M. M. Zhen, G. Li, X. Z. Liu, X. Y. Wang, C. Y. Shu, L. Jiang and C. R. Wang, *J. Mater. Chem. A*, 2013, **1**, 8105-8110.
- L. Ren, K. S. Hui and K. N. Hui, *J. Mater. Chem. A*, 2013, **1**, 5689-5694.
- S. Zhang, Y. Y. Shao, H. G. Liao, M. H. Engelhard, G. P. Yin and Y. H. Lin, *ACS Nano*, 2011, **5**, 1785-1791.
- B. Adhikari, A. Biswas and A. Banerjee, *ACS Appl. Mater. Interfaces*, 2012, **4**, 5472-5482.
- K. S. Hui, K. N. Hui, D. A. Dinh, C. H. Tsang, Y. R. Cho, W. Zhou, X. T. Hong and H. H. Chun, *Acta Materialia*, 2014, **64**, 326-332.
- D. A. Dinh, K. S. Hui, K. N. Hui, Y. R. Cho, W. Zhou, X. T. Hong and H. H. Chun, *Appl. Surf. Sci.*, 2014, **298**, 62-67.
- J. Chen, K. X. Sheng, P. H. Luo, C. Li and G. Q. Shi, *Adv. Mater.*, 2012, **24**, 4569-4573.
- S. B. Ye, J. C. Feng and P. Y. Wu, *ACS Appl. Mater. Interfaces*, 2013, **5**, 7122-7129.
- J. X. Zhu, D. Yang, X. H. Rui, D. Sim, H. Yu, H. H. Hng, H. E. Hoster, P. M. Ajayan and Q. Y. Yan, *Small*, 2013, **9**, 3390-3397.
- H. Wang, G. Wang, Y. Ling, F. Qian, Y. Song, X. Lu, S. Chen, Y. Tong and Y. Li, *Nanoscale*, 2013, **5**, 10283-10290.
- M. Sawangphruk, A. Krittayavathananon and N. Chinwipas, *J. Mater. Chem. A*, 2013, **1**, 1030-1034.
- G. Z. Hu, F. Nitze, T. Sharifi, H. R. Barzegar and T. Wagberg, *J. Mater. Chem.*, 2012, **22**, 8541-8548.
- Y. L. Wang, Y. Q. Zhao, C. L. Xu, D. D. Zhao, M. W. Xu, Z. X. Su and H. L. Li, *J. Power Sources*, 2010, **195**, 6496-6499.
- U. M. Patil, J. S. Sohn, S. B. Kulkarni, H. G. Park, Y. Jung, K. V. Gurav, J. H. Kim and S. C. Jun, *Mater. Lett.*, 2014, **119**, 135-139.

33. H. Hei, H. He, R. Wang, X. Liu and G. Zhang, *Soft Nanosci. Lett.*, 2012, **2**, 34-40.
34. X. H. Sun, H. Y. Peng, Y. H. Tang, W. S. Shi, N. B. Wong, C. S. Lee and S. T. Lee, *J. Appl. Phys.*, 2001, **89**, 6396-6399.
35. H. N. Lim, N. M. Huang, S. S. Lim, I. Harrison and C. H. Chia, *Int. J. Nanomed.*, 2011, **6**, 1817-1823.
36. B. J. Hu, T. B. Wu, K. L. Ding, X. S. Zhou, T. Jiang and B. X. Han, *J. Phys. Chem. C*, 2010, **114**, 3396-3400.
37. K. R. Priolkar, P. Bera, P. R. Sarode, M. S. Hegde, S. Emura, R. Kumashiro and N. P. Lalla, *Chem. Mater.*, 2002, **14**, 2120-2128.
38. Q. Bao, K. N. Hui, K. S. Hui, Y. Wang and X. Hong, *Mater. Res. Bull.*, 2014, **56**, 92-97.
39. W. Alhalasah and R. Holze, *J. Solid State Electrochem.*, 2007, **11**, 1605-1612.
40. R. C. Cerritos, M. Guerra-Balcazar, R. F. Ramirez, J. Ledesma-Garcia and L. G. Arriaga, *Mater.*, 2012, **5**, 1686-1697.
41. Y. X. Chen, A. Lavacchi, S. P. Chen, F. di Benedetto, M. Bevilacqua, C. Bianchini, P. Fornasiero, M. Innocenti, M. Marelli, W. Oberhauser, S. G. Sun and F. Vizza, *Angew. Chem. Int. Ed.*, 2012, **51**, 8500-8504.
42. J. Z. Sun, Y. Z. Wang, C. Zhang, T. Y. Kou and Z. H. Zhang, *Electrochem. Commun.*, 2012, **21**, 42-45.
43. Y. Wang, Y. Zhao, W. T. He, J. Yin and Y. Q. Su, *Thin Solid Films*, 2013, **544**, 88-92.
44. S. Y. Shen and T. S. Zhao, *J. Mater. Chem. A*, 2013, **1**, 906-912.